Int. J. Heat Mass Transfer. Vol. 27, No. 4, pp. 573–585, 1984
Printed in Great Britain

0017-9310/84 $3.00 + 0.00

SIZE AND NUMBER DENSITY CHANGE OF DROPLET POPULATIONS ABOVE A QUENCH FRONT DURING REFLOOD

R. LEE and J. N. REYES
Office of Nuclear Regulatory Research, U.S. Nuclear Regulatory Commission, Washington, DC 20555, U.S.A.

and

K. ALMENAS
Department of Chemical and Nuclear Engineering, University of Maryland, College Park, MD 20742, U.S.A.

(*Received* 13 *July* 1982 *and in revised form* 27 *July* 1983)

Abstract—The 'precursory cooling' in the immediate region above the quench front cannot be adequately explained using a three component (wall–droplet–vapor) phenomenological heat transfer analysis based on a single averaged droplet size. This phenomenon can be attributed to the fact that two distinct droplet generation mechanisms are present (fragmentation of bubble film and hydrodynamic) leading to a bi-spectral droplet population. A model is proposed to describe the bi-spectral droplet generation mechanism. The evaporation rate of these droplet populations is analyzed by taking into account the relevant convective and radiative heat transfer mechanisms. The rapid evaporation and diminution of the small droplet spectrum can explain the exponential rate of energy transfer from the cladding surface in the vicinity above the quench front, and by analogy the enhanced heat transfer rate downstream of flow restrictions.

NOMENCLATURE

a dimensionless parameter used in the upper limit log normal distribution or used in equation (6)
A_d cross sectional area of droplet [m^2]
B mass transfer number or blowing factor, equation (18) [dimensionless]
C_d drag coefficient [dimensionless]
D droplet diameter [μm]
D_{eq} equivalent diameter of channel [m^2]
D_{max} maximum droplet diameter [μm]
$D_{m,n}$ generalized droplet diameter,

$$\left[\int_0^\infty D^m f(D)\,dD \Big/ \int_0^\infty D^n f(D)\,dD\right]^{1/(m-n)} [\mu m]$$

e_{b_λ} emissive power [W m^{-2}]
$f(D)$ upper limit log normal distribution
F_{CD} geometric view factor between a right circular cylinder and a sphere [dimensionless]
g gravitational constant [m s^{-2}]
h_g enthalpy of steam [kJ kg^{-1}, J kg^{-1}]
h_l enthalpy of liquid [kJ kg^{-1}, J kg^{-1}]
h_{lg} $h_g - h_l$ [kJ kg^{-1}, J kg^{-1}]
i_w radiant heat flux from surface [W m^{-2}]
i'_w as defined in equation (A2) [W m^{-2}]
k conductivity [W m^{-1} K^{-1}] or Boltzmann constant
ΔL liquid film thickness of bubble [μm]
m_d mass of droplet [kg]
m''_d mass flux of evaporating droplet [kg m^{-2}]
Nu Nusselt number [dimensionless]
P pressure [MPa, psia]
Pr Prandtl number [dimensionless]
q'' heat flux [W m^{-2}]
$q_{c,r}$ convective/radiative heat flux [W m^{-2}]
Q_r radiant heat transfer rate [W]
Q_{abs} absorption coefficient of droplet [dimensionless]
r_d radius of droplet [μm]
R radius of bubble [μm]
Re Reynolds number [dimensionless]
t time [s]
T_d temperature of droplet [°C, K]
T_{sat} saturation temperature [°C, K]
T_g vapor temperature [°C, K]
T_w cladding/wall temperature [°C, K]
ΔT $T_g - T_{sat}$ [°C, K]
u_d droplet velocity [m s^{-1}]
u_g vapor velocity [m s^{-1}]
Δu $u_g - u_d$ [m s^{-1}]
v volume fraction of droplets having a diameter D
V volume of droplet [m^3].

Greek symbols

α_g steam absorptivity [dimensionless]
ε emissivity [dimensionless]
ε_g emissivity of vapor [dimensionless]
λ wavelength [μm]
ν kinematic viscosity [m^2 s^{-1}]
ρ_g density of vapor [kg m^{-3}]
ρ_l density of liquid [kg m^{-3}]
σ Stefan–Boltzmann constant [W m^{-2} K^{-4}] or surface tension [N m^{-1}].

INTRODUCTION

THE THEORETICAL study of droplet heat transfer and droplet deposition on surfaces in dispersed flow is of importance in analyzing liquid fuel spray combustion, evaporators, spray cooling and in a variety of other analyses. Among the areas of applicability, however, the greatest safety implications lie in the analysis of nuclear power reactor core coolability subsequent to a large break loss-of-coolant accident. As a result of this interest, heat transfer models employed to analyze reflood conditions have progressed from empirical correlations to a mechanistic analysis of the various heat transfer components which contribute in parallel or in series to rod quenching and the dispersed flow cooling process. Quite often the mechanistic modeling of a single process pointed out the need to model other simultaneously occurring processes. The comparison of early conduction models to experimental data revealed the need to include 'precursory cooling' immediately above the quench front. At large distances above the quench front, theoretical and experimental analysis showed that the flow is in a highly thermal non-equilibrium stage. Improvement in the temperature measurement of the superheated vapor allowed a quantitative formulation of the three component, wall–vapor–droplet, heat transfer process. A number of studies incorporating some of these simultaneously occurring heat transfer processes are available. Though different in detail, most share a highly simplified formulation for the liquid phase (i.e. droplets) in the dispersed flow. Generally it is assumed:

(1) All droplets can be represented by a single average diameter. This average drop diameter diminishes through evaporation as the flow proceeds up the channel but the number flux of these droplets remains constant.

(2) Direct wall-to-droplet heat transfer due to impingement is a minor heat transfer component and can be neglected. The inclusion of this component was evaluated by subtracting the competing (radiative and convective) heat transfer rates from the overall experimentally measured rate and was found to be fairly small.

The objective of this study is to relax the simplification made on the liquid phase of the dispersed flow and to consider all heat transfer processes simultaneously. This study will examine the droplet generation mechanism and the droplet size spectrum at the quench front and the heat transfer between the wall–vapor–droplet for the range of parameters encountered during reflood.

BACKGROUND

Dispersed flow heat transfer analysis has evolved from empirical correlations to more elaborate phenomenological studies. Most empirical studies are based on a variation of the Dittus–Boelter type turbulent single phase forced convection relationship (i.e. $Nu = c\,Re^a\,Pr^b$) [1, 2]. Two-phase flow is taken into account by modifying single phase correlations with two-phase multipliers [3, 4]. Since empirical correlations give very little physical insight regarding the nature of the dispersed flow heat transfer, researchers have undertaken a number of phenomenological studies.

The role that droplets play in dispersed flow heat transfer

Early dispersed flow models assumed thermodynamic equilibrium conditions between liquid and vapor phases [3, 5, 6]. This in effect maximized droplet importance by assuming instantaneous and complete heat and mass transfer between the droplets and the vapor. For such conditions, droplet population characteristics are irrelevant and none were considered.

The effect of droplet evaporation is included indirectly in some conduction controlled rewetting models. Thus in order to achieve better agreement with experimental values, Dua and Tien [7] proposed an exponentially decreasing 'precursory cooling' function immediately above the quench front. In experiments performed by Parker and Grosh [8], droplets were directly observed even at conditions for which equilibrium quality should exceed unity. Subsequent experimental work aided by improved instrumentation demonstrated that a large degree of superheat can be present for typical core recovery conditions [9, 10]. The extensive FLECHT experiments series [11–13] demonstrated that for the entire probable range of core reflood conditions, the superheated steam above the quench front will co-exist with dispersed liquid water. A dispersed, non-equilibrium flow regime has thus been shown to be the rule rather than the exception.

A number of investigations have subsequently proposed phenomenological and empirical correlations to describe the heat and mass transfer under such conditions [13–18]. Phenomenologically the total energy balance is usually broken down into three transfer processes as:

(1) Wall-to-vapor heat transfer (convective and radiative).

(2) Wall-to-droplet heat transfer (radiative and droplet impingement).

(3) Vapor-to-droplet heat transfer (convective and radiative).

The models differ in the importance that they assign to the droplet-to-wall heat transfer process and in the treatment of the radiative heat transfer. In most cases, both phenomena are considered to be small and are neglected. An additional and important difference is the manner by which the dispersed phase is modeled.

Chen *et al.* [14] utilized empirical correlations to determine both the drop size and the void fraction. Sun *et al.* [15] reversed the customary calculation process, that is, they treated the nature of the dispersed phase as an unknown and used an experimentally determined

heat transfer coefficient to fix the probable droplet diameter.

A phenomenological approach was proposed by Saha *et al.* [16]. The conditions of the dispersed phase were determined at the quench front, then their evolution downstream was followed through an energy and mass balance. However, as will be shown later, the mechanism chosen for droplet generation was not valid at the quench front.

A complete, three component energy transfer model was developed by Koizumi *et al.* [17], in order to analyze experimental dispersed flow data obtained by the same authors [18]. The fluid employed was not water and the droplet generation mechanism was found to be different above the quench front, but the analysis included an evaluation of the wall-to-drop heat transfer term. For experimental conditions the term was shown to be small but not negligible.

Of special importance is the experimental and associated analytical work presented in the FLECHT report series. In the earlier series [11, 12], energy transfer rates were obtained directly from energy and mass balances based on locally measured conditions. This required only integral values (i.e. local quality) for the dispersed liquid, and estimates of droplet sizes were used only in order to calculate the relatively small radiation heat transfer term. Wong [19] solved the vapor temperature distribution in a more detailed fashion by taking into account bundle geometry, axial and radial variation of vapor temperature and flow properties, and the enhancement of heat transfer due to turbulence. The droplet size and the motion of the droplets in the vapor phase was deduced from the FLECHT experimental data. In the later series [13] extensive direct measurements of the droplet population size and velocity range have been obtained and are used to modify the computational model.

Droplet creation mechanism

The coolability of a hot surface by steam carrying entrained droplets is of importance in industrial applications such as spray cooling, steam turbine and steam generator design. This diversity is noted since it is customary to consider the flow regimes encountered by the above applications as basically identical. That is, they are assumed to differ only in quantitative aspects such as quality, pressure and the average diameter used to characterize the droplet population. However, such an analogy can be made only for conditions for which the droplet population is generated by the same mechanism. The droplets of such populations would be expected to be clustered around a characteristic mean in a distribution which reflects the degree of randomness inherent in the production process and the evolution of the population during the time between production and measurement.

Therefore, in quantifying the nature of the dispersed flow regime above the quench front, the first step must be an analysis of the prevailing droplet generation mechanism. In order to evaluate the droplet-to-steam heat transfer rate, properly averaged droplet diameters, droplet number density and their relative velocity with respect to the vapor are required. Until very recently no direct measurements of these indices were available and even the latest published experimental droplet indices [13] apply only to a portion of the total droplet population. Faced with this situation, investigators have tried a number of approaches. The methods used can be divided into the following categories:

(1) Energy and mass balances (based on measured local conditions) are coupled with empirical slip correlations to define local droplet densities [11, 12].

(2) Droplet size indices are adjusted to fit experimental total heat transfer rates [15, 20].

(3) Droplet population indices measured for steady state annular flow conditions are adopted [17].

(4) Size indices are based on some postulated droplet creation mechanism. Density indices are obtained from energy and mass balances [16].

Approaches (1) and (2) are applicable primarily in the analysis and interpretation of experimental data and are unsuited for *a priori* calculations. Approach (3) could be termed the classical heat transfer method; that is, if data specific to given conditions does not exist, use available data for analogous conditions. Applicability then depends upon the choice of a proper analogy. Even superficial analysis shows that there is very little similarity between conditions above a quench front and those encountered in annular flow. The vapor above the quench front is superheated and, as it moves upward it is accelerating due to droplet evaporation and heating by the rods. In annular flow, the vapor is in thermodynamic equilibrium with the liquid phase and usually moves at a reasonably constant rate. Even more important, empirical correlations describing the droplet population in annular flow represent a kinematic equilibrium state between two competing mechanisms; entrainment due to shear forces between a faster moving liquid core and a surrounding liquid film and de-entrainment due to turbulent diffusion and gravity. Clearly, neither of these mechanisms can be postulated for conditions above the quench front. Similar objections can be raised against the use of annular flow empirical slip or void fraction correlations.

Approach (4) is thus the only consistent phenomenological method that remains; that is, the droplet population must be defined at its point of origin, the froth front, and subsequently its evolution must be followed utilizing applicable energy and mass transfer processes. This approach has been tried by several investigators. However, in most cases the mechanism chosen to generate the droplets at the froth front are of questionable validity. The mechanisms used to date can be divided into two categories:

(a) Weber number breakup [11, 12, 21],
(b) hydrodynamic film vapor interaction [16].

The Weber number breakup mechanism postulates

that for given flow conditions, there is a maximum size beyond which a droplet becomes unstable and breaks up. Such critical Weber numbers range from approximately 7 to 12. At best this approach can define only the upper size limit for a droplet population. However, for many flow conditions, such criterion could not even give the correct size range [22].

The importance of annular flow and droplet entrainment from liquid surfaces has led to the postulation of a number of entrainment mechanisms and associated empirical entrainment correlations. Examples of such mechanisms are the Kelvin–Helmholtz [23], the Roll Wave [24] and Wave Undercut [25]. Applicability of a given mechanism depends primarily on the thickness turbulence level of the available liquid layer, but they all depend on momentum transfer from a fast moving vapor stream to a slower moving or stationary liquid surface. If such shear flow conditions do not exist then clearly the above mechanisms cannot be applied.

DROPLET FORMATION MECHANISM AND DROPLET SIZE SPECTRA ABOVE A QUENCH FRONT

In a restricted sense the quench front is the region on the cladding surface where initial continuous contact between liquid and cladding is established. There is a narrow zone of violent film boiling immediately downstream of it and a wider region of strong nucleate boiling below. The vapor generated by this boiling is released into the fairly crowded ($D_{eq} = 0.01$ m) inter-rod channel. This produces a continuously rising stream of bubbles that merge into a foamy layer. Observations and photographic evidence [26] have shown that this foamy region oscillates substantially about the quench front and it is within this region that the droplets originate. As shown in Fig. 1, two distinct mechanisms for the generation of droplets exist, giving rise to two separate droplet populations. These are:

(1) A population of quite small droplets (10–50 μm)

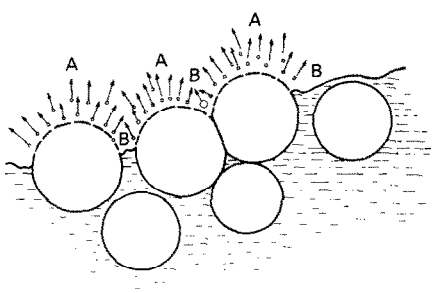

FIG. 1. Droplet creation mechanisms above a quench front.

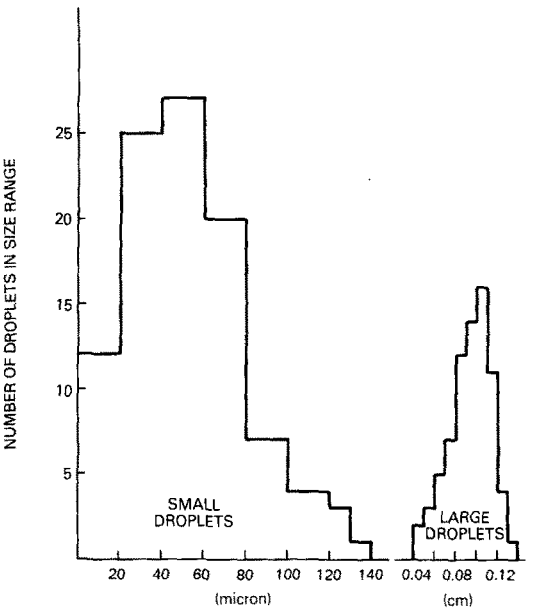

FIG. 2. Histograms showing size distribution of large and small droplets resulting from bubble burst mechanism from Newitt *et al.*'s experiment [29].

is produced by the fragmentation of the bubble film. The size of these droplets will be characterized by the thickness of the bubble film.

(2) A population of much larger droplets formed from the interstitial water which is being swept upward with the foam. It is this droplet population which is measured at the observation point. Average measured or inferred diameters range from 400 to 1200 μm [27, 28].

Bubble burst mechanism

Droplet generation by the bubble burst mechanism has been investigated by Newitt *et al.* [29]. In their experiment, air bubbles were released under a quiescent liquid surface. A typical histogram showing size distribution of the generated large and small droplets is shown in Fig. 2. Two distinct populations were observed. A large population of quite small droplets (average diameter of 30–35 μm) produced by the fragmentation of the bubble film. The average size of these drops decreased with increasing water temperature. A less numerous population of large drops (average diameter of 1000 μm) was produced by a surging flow of water into the depression left after the bubble has burst. The ratio of the number of small to large droplets ranged from 1 to 100 and increased strongly with increasing bubble diameter. It seemed to have no correlation with temperature.

Above a quench front the generation mechanism of the large bubbles is different, but the fragmentation of the bubble film is entirely analogous. Thus if differences in water temperature are taken into account, the small droplet measurements are directly applicable. Quench front bubble diameters are restricted by inter-rod distances and thus should not exceed ~0.4 cm.

However, the temperature conditions are different. Newitt *et al.* varied liquid temperatures within a fairly narrow range (from 25 to 45°C) while quench front liquid would be expected to be in the range of 108–145°C. Both surface tension and viscosity change appreciably in this temperature interval and this would be expected to influence the thickness of the liquid bubble film and consequently the size of the fragmented drops. For the dynamic conditions existing for a rising and bursting bubble, film thickness should vary inversely with surface tension and directly with liquid viscosity. The surface tension film squeezes the trapped water which flows laminarly to the sides. A bubble with constant surface tension is therefore not stable and bursts quickly. The amount of water squeezed out in this transient time should be proportional to the pressure driving force (the surface tension) and inversely proportional to viscosity. Droplet size is then proportional to the water remaining in the liquid film. Employing the noted assumptions, a temperature shift from 45 to 145°C results in a diameter multiplication factor of 0.58 as shown in ref. [30]. Based on the previous reasoning and Newitt *et al.*'s data, the expected $D_{1,0}$ diameter for droplets produced by film fragmentation above the quench front is approximately 30 μm.

As noted the generation mechanism of large droplets in Newitt *et al.*'s experiments is quite different and no direct correlation with quench front conditions should be expected. Above the quench front large droplets are created when interstitial water collected between several simultaneously rising bubbles is hurled into the accelerating vapor region. The droplets formed can be quite large, therefore surviving the transition from the quench front to the measurement location with relatively little decrease in diameter due to evaporation.

Careful measurement of droplet size for a range of reflood conditions have been made during the FLECHT–SEASET tests. The measured distributions are presented in ref. [13], in terms of lower limit log normal distributions. While producing satisfactory indices, such a distribution unduly weights the upper range of the population. As long as the droplets do not evaporate completely this is of small consequence. However, for complete evaporation, an unrealistically long time for evaporation of the entire population will be calculated. For this reason, the data for both the large and small droplet populations have been re-correlated on the basis of the upper limit log normal distribution. As shown in Fig. 3, this produces a reasonable fit for the large droplet spectrum.

The utilization of Newitt *et al.*'s data and the available FLECHT–SEASET measurements thus define the initial size indices of both distributions. The major remaining unknown is the initial number or weight ratio between these two populations. No direct experimental data is available, thus the ratio must be established by a reasonable hypothesis. As shown in Fig. 4, the minimum number of bubbles between which interstitial liquid can be trapped is three. In the restricted inter-rod space this will probably be the dominant mode of large drop generation. The volume of interstitial liquid can then be established by geometric arguments. It is further assumed that only half of the liquid in the liquid film generates small droplets, the other half is retracted into the foam front by surface tension. Based on the model, if the liquid film thickness is known, one can estimate the weight or number ratio between the large and small droplet populations. From studies of thinning of liquid film, the minimum thickness is estimated to be in the order of 200 Å with an average thickness of 1000 Å [31]. Typical small and large droplet spectrums generated by the assumed model during a 0.12 s integral period are shown in Fig. 5. The very high evaporation rate of the small droplet population altered their number density even in this short time interval. Figure 5, therefore, also shows a calculated instantaneous distribution.

Table 1. Conditions above quench front measured and predicted in the FLECHT–SEASET experiment series

Parameters	Range of conditions
Cladding temperature	437–1490 K
Vapor temperature	393–1393 K
System pressure	0.138–0.414 MPa
Core inlet water velocity	0.01–0.15 m s^{-1}
Core inlet mass flux	9.2–142.8 kg m^{-2} s^{-1}
Duration of rod uncovery	35–960 s
Void fraction	0.7–1.0
Vapor velocity†	3–18 m s^{-1}
Quality:†	
equilibrium	0.4–1.42
actual	0.4–0.7

† Predicted.

DROPLET EVAPORATION

Above the quench front, droplets are hurled into the vapor space with varying degrees of initial momentum and a distribution of initial directions. As they move up the channel the ambient conditions will vary strongly with position and time. Just ahead of the quench front the vapor temperature will be close to saturation and the clad surface temperature can lead it up to 800 K. The ambient temperature then rises very rapidly and the vapor accelerates due to thermal expansion and the additional vapor created by the rapid evaporation of the smaller droplets. The droplets thus find themselves in a highly superheated and continuously accelerating environment. Their size and number density distribution will change due to evaporation, coagulation and droplet breakup. The latter two mechanisms will be especially important and dominant at channel locations where changes in vapor momentum occur, such as at grid spacers or in channel restrictions due to clad ballooning. At these locations the droplet distribution is modified by the creation of an additional small droplet population due to impingement breakup and shattering of the larger droplets. This effect is

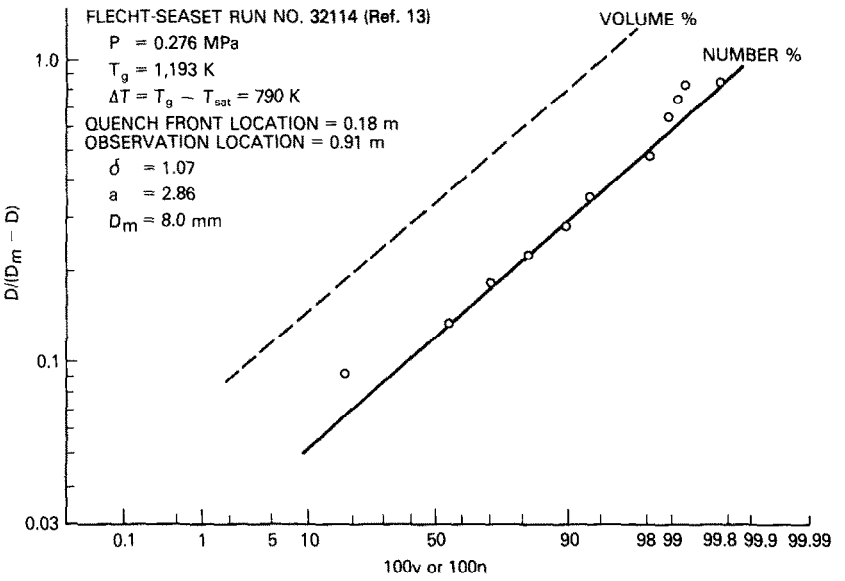

FIG. 3. $D/(D_m - D)$ as a function of cumulative volume or number percentage.

usually strong enough to produce local desuperheating and thus a measurable decrease in adjacent clad temperature [32]. In this respect the region immediately above a restriction resembles the region above the quench front. That is, in both cases a transient, quickly evaporating small droplet population is present.

In this study the droplet population evolution in the path segment between the quench front and the first channel restriction is considered. The results are also qualitatively applicable to path segments between sequential restrictions. The predominant droplet population evolution mechanism in such straight path segments is evaporation in a highly superheated vapor with a radiant heat transfer component contributed by the high surface temperatures of the surrounding rods.

Droplet evaporation model

The calculation model employed integrates the momentum, energy and mass balance equations using a finite-difference predictor–corrector method and a variable time step chosen by the program to assure a specified accuracy. Initially, the droplet is assumed to be stationary, it accelerates under the influence of gravity, reaches some maximum velocity, then decelerates as the decreasing droplet radius increases

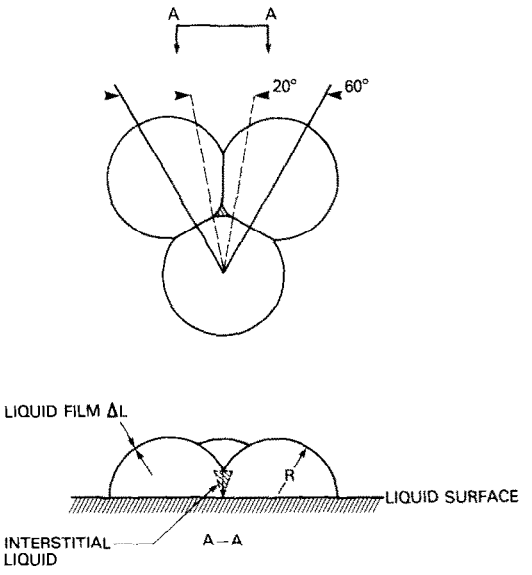

FIG. 4. Model for quantifying large to small droplet weight ratio.

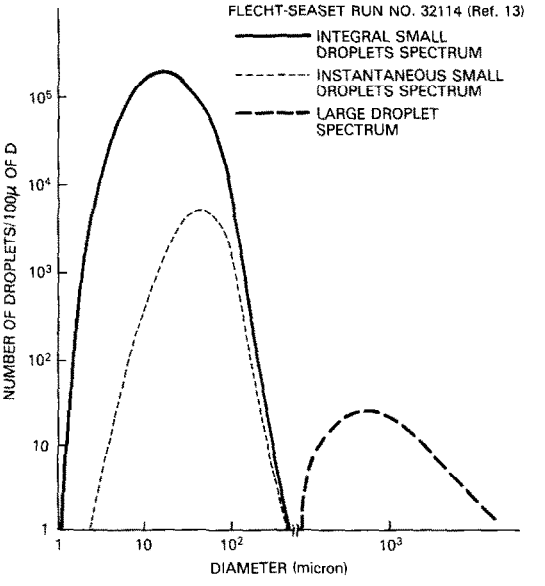

FIG. 5. Number of small and large droplets generated during a 0.12 s interval.

the importance of the frictional drag term. Ambient conditions are assumed to be constant and are chosen to span the condition range expected above the quench front. Both radiative and convective heat transfer is considered.

The time-dependent momentum balance equation for a droplet expresses the balance of gravity, drag and buoyancy forces as

$$m_d \, du_d/dt = 1/2 * C_d A_d \rho_g (u_g - u_d)^2 - g(\rho_l - \rho_g). \quad (1)$$

Solving for the acceleration of the drop

$$d(\Delta u)/dt = g(\rho_l - \rho_g) - 3/8 * C_d \rho_g (\Delta u)^2/(\rho_l r_d), \quad (2)$$

where C_d is a function of Reynolds number and is given by

$$C_d = 24/Re, \qquad Re < 53,$$
$$= 0.45, \qquad Re > 53. \quad (3)$$

Note that equation (2) represents the acceleration of the droplet relative to the surrounding vapor. The relative velocity is required to evaluate the droplet Reynolds number.

The droplets generated above the quench front are at saturation temperature, thus the entire energy transferred to the droplet serves to evaporate it. Combining the mass and energy balance equations yields the mass flux per droplet

$$dm_d''/dt = q''/h_{lg}, \quad (4)$$

where q'' incorporates both convective and radiative heat transfer components. That is

$$q'' = q_c'' + q_r''. \quad (5)$$

The methodology used to evaluate the radiant heat transfer component is presented in the Appendix.

For a sphere in free motion, the average Nusselt number for convective heat transfer takes the form

$$\overline{Nu} = 2.0 + a \, Re^{1/2} \, Pr^{1/3}. \quad (6)$$

Customarily the Ranz–Marshall [33] correlation is used which sets $a = 0.6$, however, experiments performed by Lee and Ryley [34] have shown that for superheated vapor conditions the value of $a = 0.74$ is preferable.

It has been shown that at high evaporation rates the evaporation from the droplet reduces convective heat transfer from vapor to the droplet [35, 36]. This is due to the fact that the vapor mass flux leaving the surface of the droplet flows countercurrent to the heat flux. In order to incorporate this effect, the average Nusselt number is corrected by the blowing factor, $(1 + B)$

$$\overline{Nu}(1 + B) = 2.0 + 0.74 Re^{1/2} \, Pr^{1/3}, \quad (7)$$

where B is the mass transfer number defined as

$$B = \frac{h_g(T_g) - h_l(T_d)}{h_g(T_d) - h_l(T_d)}. \quad (8)$$

Using Nu from equation (7), the convective heat flux is given by

$$q_c'' = \overline{Nu} \, k(T_g - T_d)/D. \quad (9)$$

The droplet population, D, has to be replaced by an appropriately weighted average. The weighting procedure for various evaporation regimes is outlined in ref. [30].

CALCULATIONAL RESULTS

The outlined model has been employed to calculate droplet evaporation rates for the range of conditions expected above the quench front. The initial droplet radius and the vapor temperature and pressure were treated as independent variables. A linear relationship [30] with the superheated vapor temperature is used to determine rod clad temperature. Figure 6 shows typical life histories for representative droplet sizes at a vapor temperature of 840°C and ΔT of 732°C, and a pressure

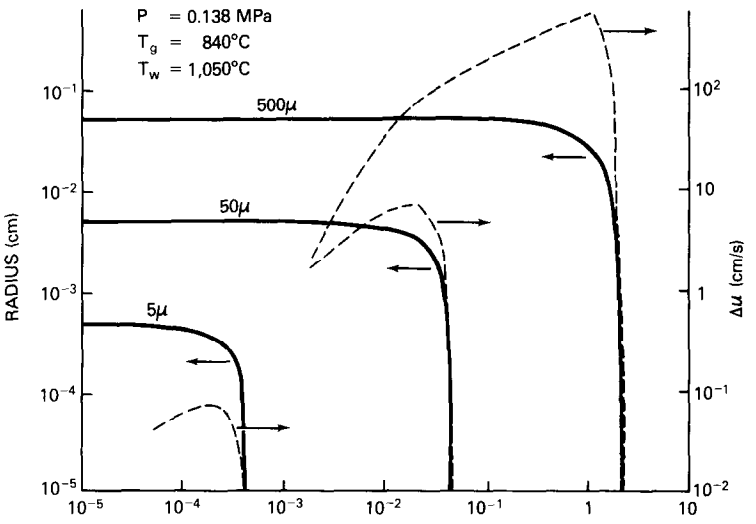

FIG. 6. Life histories of evaporating droplets of different sizes.

of 0.138 MPa (20 psia). The solid line represents the droplet radius; the dashed line, the vapor-to-droplet relative velocity. The life history of a droplet can be followed by noting the velocity trace of the 500 μm droplet. The droplet accelerates first in laminar flow, then (after ~ 0.02 s) in turbulent flow till it reaches a maximum relative velocity of 6 m s^{-1} at 1.5 s. Droplet evaporation and diminution in size leads to a relative increase in the drag coefficient. As its size decreases further, its relative velocity decreases as well, and the droplet evaporates completely in 2 s. A similar life history is repeated, but in a considerably shorter time for the smaller droplets. Thus a 50 μm droplet and a 5 μm droplet evaporate in 0.05 s and 0.5 ms, respectively. The calculated droplet lifetime history for the entire range of conditions above the quench front is summarized in Figs. 7 and 8. The strong dependence of evaporation time on the initial drop diameter displayed by the figures can be used to estimate evaporation distances for the two separate drop populations.

The distance between spacers and thus the maximum distance that can exist between the quench front and the nearest spacer is ~ 1 m. The velocity shown in Fig. 6 is the relative velocity between the droplet and the vapor. Since the vapor velocity ranges from 3 to 5 m s^{-1}, the net velocity of the indicated droplets will be upward and they will traverse the distance towards the nearest spacer in 0.06–0.3 s with typical transit time being ~ 0.12 s. It should be noted that actual, evaporating conditions for a droplet above a quench front will vary with time and position. A droplet is likely to start out with some initial relative velocity imparted by the bursting bubble. Near the quench front the vapor temperature will be close to saturation, and the wall temperature will lead it substantially. The vapor increases in temperature and accelerates due to the thermal expansion and droplet evaporation as the droplet proceeds up the channel. Nevertheless, for the respective droplet populations, the evaporation times differ so substantially that definite conclusions concerning their evolution can be drawn. These can be summarized as follows:

(1) For the entire range of conditions above the quench front, the small droplet population will evaporate entirely within a distance of 10–50 cm above the quench front.

(2) Except for the small vapor velocities (low power and low reflood rate), the large droplet population will be changed relatively little.

This implies that the droplet population in the immediate quench front region and an appreciable distance away from it (0.5 m) differs not merely quantitatively but qualitatively as well. Near the

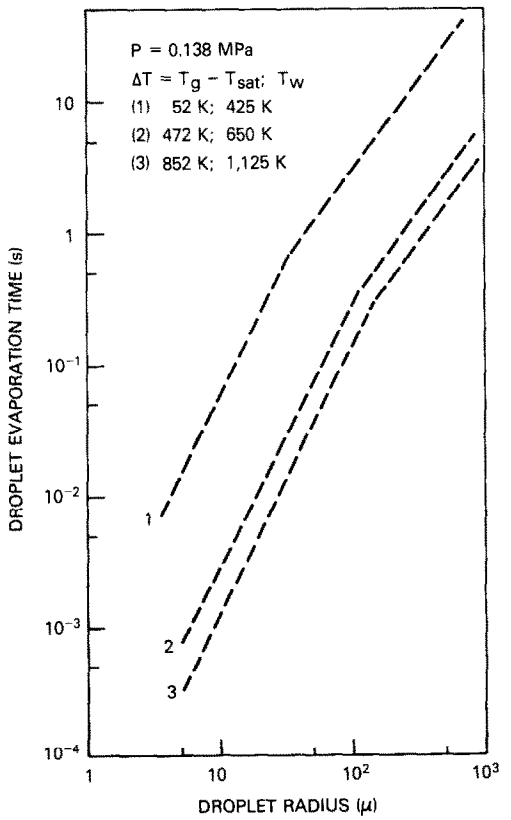

FIG. 7. Droplet evaporation time for representative conditions above a quench front as a function of droplet radius.

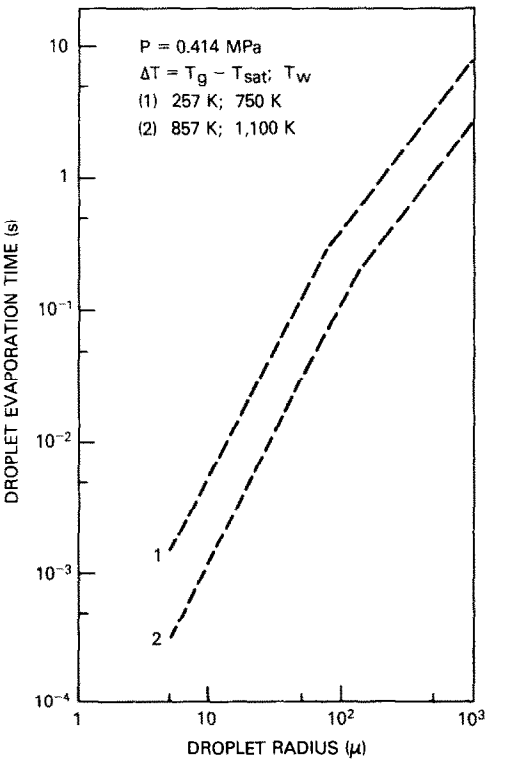

FIG. 8. Droplet evaporation time as a function of droplet radius.

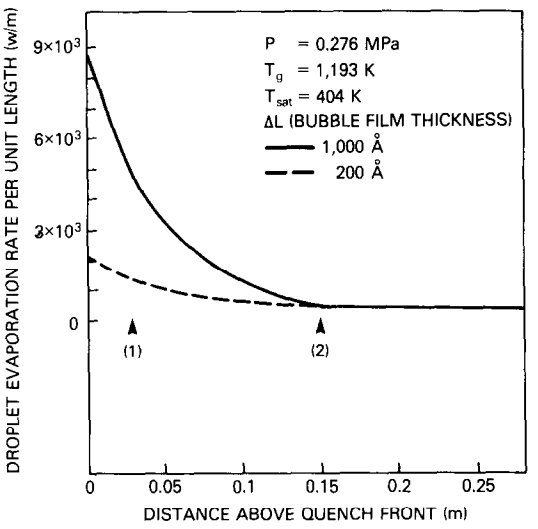

(1) PROBABLE EXTENT OF QUENCH FRONT FROTH LEVEL
(2) PROBABLE DISTANCE OF SMALL DROPLET PENETRATION

FIG. 9. Droplet evaporation rate per unit length as a function of distance above the quench front.

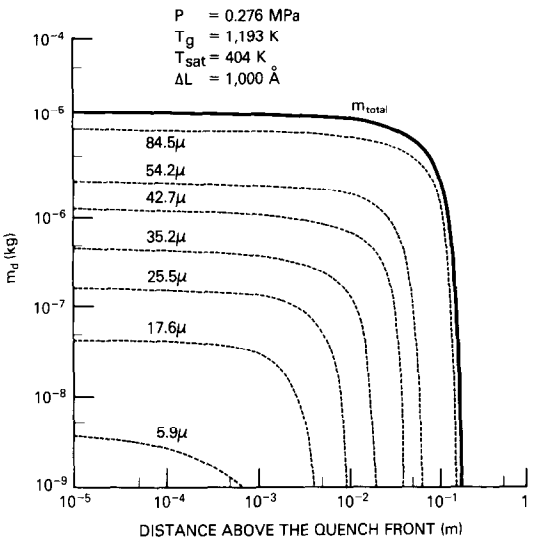

FIG. 10. Evaporation of small droplet spectrum as a function of the distance above the quench front.

quench front it is a bi-spectral distribution characterized by a large but rapidly diminishing number of small droplets. At a distance from the quench front it evolves into a numerical relatively stable population of large droplets which are slowly diminishing in size. This is contrary to several post quench front heat transfer models which assume a numerically stable droplet population [16, 27].

The significance of the two droplet population model is illustrated in Fig. 9 which displays a calculation of the energy absorption rate by the droplets as a function of distance above the quench front. Two values of the bubble film thickness are chosen in order to estimate the weight ratio of the small to large droplet populations. The actual small population weight fraction is thus bracketed by the indicated limits. The results presented serve to explain the heat transfer phenomena observed above the quench front and by analogy above the grid spacers or rod channel restrictions. As shown, although in terms of total liquid weight the small droplet population represents a seemingly minor fraction (i.e. 1–5%) at the point of origin, their extremely rapid rate of evaporation will dominate the local energy transfer rates. The presence of the small droplet population will in effect create a qualitatively different, rapidly changing heat transfer zone.

The spatial evolution of the smaller droplets is shown in more detail in Fig. 10 which presents the evaporation history of individual groups of the small droplets above the quench front. As one can observe, for the smallest drops ($D < \sim 10$ μm), evaporation rates are so rapid that droplets evaporate essentially within the diffuse quench front and contribute to the general two-phase film boiling heat transfer which characterizes this region. Droplets having larger radii have sufficiently long lifetimes to join the continuous vapor region above the quench front. They evaporate at various distances above the front. The diminution of the number density of the small droplet population and thus its energy absorption rate, decreases in an approximately exponential manner above the quench front. This computational result provides a phenomenological basis for some analytical models and aids in quantifying observed experimental data. Thus Dua and Tien [7] in developing a conduction controlled quench front propagation model found that the inclusion of an exponentially decreasing 'precursory cooling' term above the quench front improved agreement with experimental results. The enhanced heat transfer rate above flow channel restrictions has been measured by several experiments [32, 37]. As noted, channel restrictions have a qualitative similarity to a quench front in the sense that both serve as generation sites for a small droplet population. The evaporation of this small droplet population then locally desuperheats the vapor and leads to a notable increase in the clad-to-coolant heat transfer rate. Obtained measurements agree quantitatively with the calculated results of Figs. 9 and 10. Thus in ref. [37] it is shown that clad ballooning (an indication of high local clad temperature) occurs preferentially ~20–30 cm downstream from grid spacers. Direct measurements of clad and vapor temperatures show that the decrease of local temperature persists for ~10–20 cm beyond a restriction.

CONCLUSION

A review of the literature has indicated that a satisfactory model of the mechanism of droplet generation based on conditions near the quench front does not exist. The application of Weber number

breakup and hydrodynamic film vapor interaction for droplet generation about the quench front is shown to be invalid. In this study, it is shown that not one but two distinct droplet generation mechanisms exist at a quench front. This leads to the generation of two droplet populations having widely separated characteristic diameters and consequently radically different evaporation rates.

The population characteristics of small droplets is obtained by drawing an analogy between the small droplet generation by the bubble burst mechanism in Newitt *et al.*'s experiment and the bursting of a continuously rising stream of bubbles near the quench front. The size of these small droplets will depend on the thickness of the bubble film. It is postulated that large droplets are created when interstitial water trapped between several simultaneously rising bubbles is hurled into the accelerating vapor region.

A representative large droplet spectrum is obtained from the FLECHT–SEASET experiments. It is proposed that the initial weight ratio between the small and large droplet populations can be estimated by quantifying the liquid mass in the bubble film and the trapped liquid between simultaneously rising bubbles. From studies of thinning of liquid films, the minimum thickness is estimated to be of the order of 200 Å, with an average thickness of the order of 1000 Å. The resulting weight fraction of the small droplet population is then 0.01 and 0.05, respectively.

Droplet evaporation between the quench front and the first channel restriction is calculated by the integration of the momentum, energy and mass balance for a droplet convective and radiant heat transfer between the wall and the vapor, and the vapor and the droplet are considered. The calculated evaporation time for different droplet sizes are presented. It is found that the droplet population changes significantly between the point of creation of the droplets and the next channel restriction. The rapid evaporation and diminution of the small droplet spectrum can explain the exponential rate of energy transfer from the cladding surface in the vicinity of the quench front. By analogy the model can be used to explain the enhanced heat transfer observed downstream of channel restrictions.

REFERENCES

1. D. C. Slaughterback, L. J. Ybarrondo and C. F. Obenchain, Flow film boiling heat transfer correlations parametric study with data comparisons, ASME Paper 73-HT-50 (1973).
2. D. C. Groeneveld, Prediction of thermal non-equilibrium in the post-dryout regime, *Nucl. Engng Des.* **30,** 17–26 (1976).
3. D. C. Groeneveld, An investigation of heat transfer in the liquid deficient regime, AECL-3281, Chalk River, Ontario, Canada (1969).
4. D. N. Plummer, O. C. Iloeje, W. M. Rohsenow, P. Griffith and E. Ganic, Post critical heat flux to flowing liquid in a vertical tube, MIT Report No. 72718-91, Cambridge, Massachusetts, September (1974).
5. R. S. Dougall and W. M. Rohsenow, Film boiling on the inside of vertical tubes with upward flow of the fluid at low qualities, MIT Report No. 9079-26, Cambridge, Massachusetts, September (1963).
6. S. L. Richlen and K. G. Condie, Comparison of post-CHF heat transfer correlations to tube data, INEL, SRD-134-76, Idaho Falls, Idaho (1976).
7. S. S. Dua and C. L. Tien, Two-dimensional analysis of conduction controlled rewetting with precursory cooling, *J. Heat Transfer* **98,** 407–413 (1976).
8. J. D. Parker and R. J. Grosh, Heat transfer to mist flow, ANL-6291, Argonne National Laboratory, Chicago, Illinois, January (1961).
9. S. M. Nijhawan, J. C. Chen, R. K. Sundaram and E. J. London, Measurement of vapor superheat in post critical heat flux boiling, *J. Heat Transfer* **102,** 465–470 (1980).
10. S. M. Nijhawan, J. C. Chen and R. K. Sundaram, Parametric effects on vapor non-equilibrium in post-dryout heat transfer, ASME Paper 80-WA/HT-50 (1980).
11. G. P. Lilly, H. C. Yeh, C. E. Dodge and S. Wong, PWR FLECHT–SEASET skewed profile low flooding rate test series evaluation report, WCAP-9183, Westinghouse Electric Corporation, Pittsburgh, Pennsylvania, November (1977).
12. G. P. Lilly, H. C. Yeh, L. E. Hochreiter and N. Yamaguchi, PWR FLECHT cosine low flooding rate test series evaluation report, WCAP-8838, Westinghouse Electric Corporation, Pittsburgh, Pennsylvania, March (1977).
13. N. Lee, S. Wong, H. C. Yeh and L. E. Hochreiter, PWR FLECHT–SEASET unblocked bundle, forced and gravity reflood task: data evaluation and analysis, WCAP-9699, Westinghouse Electric Corporation, Pittsburgh, Pennsylvania, July (1980).
14. J. C. Chen, F. T. Ozkaynak and R. K. Sundaram, Vapor heat transfer in post-CHF region including the effect of thermodynamic non-equilibrium, *Nucl. Engng Des.* **51,** 143–155 (1979).
15. K. H. Sun, J. M. Gonzalez-Santalo and C. L. Tien, Calculations of combined radiation and convection heat transfer in rod bundles under emergency cooling conditions, *J. Heat Transfer* **98,** 414–420 (1976).
16. P. Saha, B. S. Shiralkar and G. E. Dix, A post-dryout heat transfer model based on actual vapor generation rate in dispersed droplet regime, ASME Paper 77-HT-80 (1977).
17. Y. Koizumi, T. Ueda and H. Tanaka, Post-dryout heat transfer to R-113 upward flow in a vertical tube, *Int. J. Heat Mass Transfer* **22,** 669–678 (1979).
18. T. Ueda, H. Tanaka and Y. Koizumi, Dryout of liquid film in high quality R-113 upflow in a heated tube, *Proc. 6th Int. Heat Transfer Conf.*, Toronto, Canada, pp. 423–428 (1978).
19. S. Wong, A model for dispersed flow heat transfer in rod bundles during reflood, Ph.D. thesis, Carnegie-Mellon University, Pittsburgh, Pennsylvania (1979).
20. R. A. Seban, R. Greif, W. Peake and H. Wong, Predictions of drop models for the dispersed flow downstream of the quench front in tube reflood experiments, ASME Paper 80-WA/HT-47 (1980).
21. G. L. Yoder, Dispersed flow film boiling, Ph.D. thesis, Massachusetts Institute of Technology, Cambridge, Massachusetts (1980).
22. T. Ueda, Entrainment rate and size of entrained droplets in annular two-phase flow, *Bull. J.S.M.E.* **22,** 1258–1265 (1979).
23. D. F. Tatterson, J. C. Dallman and T. J. Hannatty, Drop size in annular gas–liquid flows, *A.I.Ch.E. Jl* **23,** 68–76 (1977).
24. G. F. Hewitt and N. S. Hall-Taylor, *Annular Two-phase Flow*, p. 136. Pergamon Press, New York (1970).
25. W. R. Lane, Shatter of drops in streams of air, *Ind. Engng Chem.* **43,** 1312–1317 (1951).
26. V. K. Dhir, R. B. Duffey and I. Catton, On the quenching of a four rod bundle, ASME Fluid Flow and Heat Transfer

Over Rod or Tube Bundle, Winter Meeting, New York, pp. 231–238, American Society of Mechanical Engineers (1979).
27. L. E. Hochreiter, M. J. Loftus and C. E. Conway, PWR FLECHT-SEASET unblocked bundle, forced and gravity reflood task: data report, NUREG/CR-1532, U.S. NRC, Washington, DC, June (1980).
28. S. Yao and A. Rane, Heat transfer of laminar mist flow in tube, *J. Heat Transfer* **102,** 678–683 (1980).
29. D. M. Newitt, N. Dowbrowski and F. H. Knelman, Liquid entrainment: 1, the mechanism of drop formation from gas or vapor bubbles, *Trans. Instn Chem. Engrs* **32,** 244–262 (1954).
30. R. Lee, Dispersed flow heat transfer above a quench front during reflood in a pressurized water reactor after a large break loss-of-coolant accident, Ph.D. thesis, University of Maryland, College Park, Maryland (1982).
31. J. T. Davies and E. K. Rideal, *Interfacial Phenomena.* Academic Press, New York (1961).
32. L. E. Hochreiter, FLECHT-SEASET 161 unblocked bundle and 21 rod bundle flow blockage results, Paper presented at the 8th Water Reactor Safety Research Information Meeting, USNRC, Gaithersburg, Maryland, October (1980).
33. W. E. Ranz and W. R. Marshall, Evaporation from drops, Parts I and II, *Chem. Engng Prog.* **48,** 141–146, 173–180 (1952).
34. K. Lee and D. Ryley, The evaporation of water droplets in superheated steam, ASME Paper 68-HT-11 (1968).
35. M. C. Yuen and L. W. Chen, Heat transfer measurements of evaporating liquid droplets, *Int. J. Heat Mass Transfer* **21,** 537–542 (1973).
36. G. M. Harpole, Water droplet evaporation in high temperature surrounds, ASME Paper 79-WA/HT-6 (1979).
37. P. Ihle, M. Politzky and K. Rust, Flow blockage effects with by-pass, ASME/AIChE 19th National Heat Transfer Conf., Orlando, Florida, American Society of Mechanical Engineers and American Institute of Chemical Engineers (1980).

APPENDIX

RADIATIVE HEAT TRANSFER IN A ROD BUNDLE

Radiative heat transfer can significantly enhance the evaporation of droplets near high temperature surfaces. For this study, it is assumed that the droplet is located at the center of the flow channel and thus receives radiant energy from four surrounding pins. The quantity of radiative heat absorbed by the droplet will depend on the droplet size, its temperature and the wavelength of the incident energy. The droplet is immersed in a steam environment and hence its distance from the radiating surfaces must be considered. The radiative properties of the pin surfaces, the steam and the droplet must be known. For this analysis, the following assumptions regarding radiative heat transfer to a single droplet are made:

(1) The pin surface is considered to be 'gray' and 'diffuse' and the emitted energy is characterized by the wavelength of maximum intensity.
(2) Only the absorptivity and emissivity of the steam is considered.
(3) The droplet is assumed to be spherical.
(4) The geometric view factor between the four pin channel and the droplet is approximated by a right circular cylinder of equivalent hydraulic diameter radiating to a sphere.

A detailed discussion of the above four assumptions is given in ref. [30]. The total radiant flux emitted by the pin surfaces which view the droplet can be described by

$$i_w = F_{CD}(\varepsilon\sigma T_w^4 + (1-\varepsilon)\bar{\varepsilon}_g T_w^4). \quad \text{(A1)}$$

The second term on the RHS of equation (A1) describes the radiant flux reflected by the pin surfaces. The total energy flux reaching the droplet after attenuation by the surrounding steam is

$$i'_w = (1-\alpha_g)i_w, \quad \text{(A2)}$$

where α_g is the steam absorptivity. A portion of the attenuated flux can be either absorbed or scattered by the droplet. In addition, the surrounding steam is also radiating to the droplet. Taking all of these factors into account, the total energy absorbed by the droplet becomes

$$Q_r = 4\pi r^2 * Q_{abs} * (i'_w + \bar{\varepsilon}_g \sigma T_g^4). \quad \text{(A3)}$$

Therefore, q''_r is

$$q''_r = Q_{abs} * (i'_w + \bar{\varepsilon}_g \sigma T_g^4). \quad \text{(A4)}$$

The radiative heat transfer model utilized in this study incorporates details usually not considered in the literature. This was reflected in the calculated results which revealed some initially unsuspected trends. An example is shown in Fig. A1 which presents the relative importance of the radiant heat transfer term as a function of droplet radius with cladding temperature as a chosen parameter. The strong radial variation shown is a consequence of increasing convective heat transfer for smaller radius droplets. The change in the slope of this ratio occurring at a radius of 100–300 μm reflects the change in convective heat transfer produced by a transition from a predominantly laminar to a predominantly turbulent flow regime. Such trends are thus readily explained in terms of the model. More surprising is the behavior of the trace representing the higher cladding temperature used in the calculation for droplets of radius under 100 μm (lines 1 and 2). Contrary to intuition, the relative importance of the radiant heat transfer for the higher wall temperature decreases in comparison to the lowest wall temperature. The behavior could be explained by considering Fig. A2, where the normalized emissive power of the radiating cladding surface at two different temperatures of 780 and 1150°C, and the

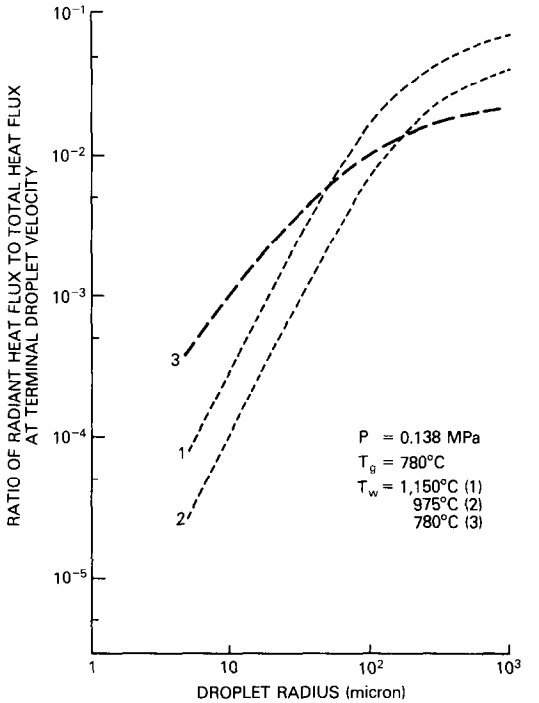

FIG. A1. Ratio of radiant heat flux to total heat flux at terminal droplet velocity as a function of droplet radius.

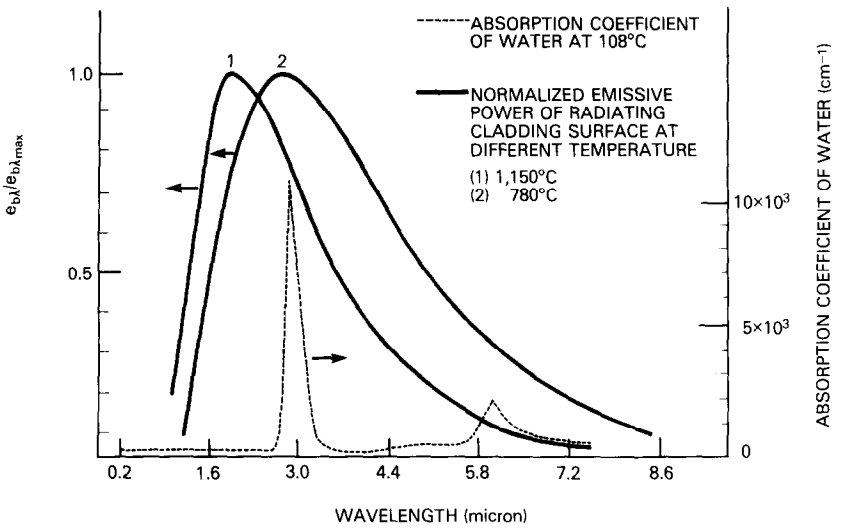

FIG. A2. Normalized emissive power of the radiating cladding surface and the absorption coefficient for water at 108°C as a function of wavelength.

absorption coefficient for water at 108°C is plotted against the wavelength. In this study, the emitted energy for the cladding surface is characterized by the wavelength at the maximum intensity. The wavelength for maximum intensity for the cladding temperature of 780°C, as shown in Fig. A2, happens to fall within the absorption peak of the water resulting in higher radiant heat transfer to the droplet. However, the wavelength for intensity for the cladding temperature of 1150°C falls outside of the absorption peak and hence results in significantly lower radiant heat transfer to the droplet.

CHANGEMENT EN TAILLE ET EN DENSITE NUMERIQUE DE POPULATION DE GOUTTELETTES AU DESSUS D'UN FRONT DE TREMPE PAR REMOUILLAGE

Résumé—Le "refroidissement précurseur" dans la région immédiate au dessus d'un front de trempe ne peut être expliqué correctement en utilisant une analyse phénoménologique à trois composants (paroi–gouttelette–vapeur) basée sur une simple taille moyenne de goutte. Ce phénomène peut être attribué au fait que deux mécanismes distincts de génération de gouttelettes (fragmentation du film de bulle et hydrodynamique) sont présents conduisant à une population bi-spectrale de gouttelettes. On propose un modèle pour décrire le mécanisme de génération bi-spectrale de gouttelettes. Le flux d'évaporation de cette population est analysé en prenant en compte les mécanismes de transfert de chaleur par convection et par rayonnement. L'évaporation rapide et la diminution du spectre des petites gouttelettes peuvent expliquer le flux exponentiel d'énergie à partir de la surface à son voisinage sous le front de refroidissement brusque, et par analogie l'accroissement du flux thermique en aval des restrictions d'écoulement.

ÄNDERUNG VON GRÖSSE UND HÄUFIGKEITSVERTEILUNG DER TROPFENPOPULATION OBERHALB EINER ABSCHRECKFRONT WÄHREND DES FLUTUNGSVORGANGS

Zusammenfassung—Die Vorkühlung unmittelbar oberhalb der Abschreckfront kann nicht angemessen durch ein phänomenologisches Dreikomponentenmodell (Wand–Tropfen–Dampf) erklärt werden, das auf einer mittleren Einzeltropfengröße basiert. Dieser Umstand kann der Tatsache zugeschrieben werden, daß zwei verschiedene Tropfenentstehungsmechanismen vorhanden sind (Zerstörung des Blasenfilms und hydrodynamische Einflüsse), die zu einer bispektralen Tropfenpopulation führen. Es wird ein Modell zur Beschreibung des bispektralen Tropfenentstehungsmechanismus vorgeschlagen. Die Verdampfung dieser Tropfenpopulationen wird unter Berücksichtigung der maßgebenden Wärmeübertragungsmechanismen von Konvektion und Strahlung untersucht. Die schnelle Verdampfung und Abnahme des Spektrums der kleinen Tropfen kann den exponentiellen Anstieg des Wärmeübergangs an der Oberfläche der Hüllrohre im Bereich unmittelbar oberhalb der Abschreckfront erklären und analog dazu den erhöhten Wärmeübergang stromabwärts von Strömungshindernissen.

ИЗМЕНЕНИЕ РАЗМЕРА И КОНЦЕНТРАЦИИ ПУЗЫРЬКОВ НАД ФРОНТОМ ЗАКАЛКИ ПРИ ПОГРУЖЕНИИ В ЖИДКОСТЬ

Аннотация—"Предварительное" охлаждение непосредственно над фронтом закалки нельзя объяснить адекватно, используя трехкомпонентный (стенка–капли–пар) феноменологический анализ переноса тепла, основанный только на усредненном размере капель. Причиной является тот факт, что здесь имеют место два различных механизма образования пузырьков (дробление пузырьковой пленки и гидродинамический), так что график функции распределения пузырьков по размерам является двугорбым. Предложена модель для описания указанных механизмов зарождения пузырьков. Скорость испарения таких пузырьковых скоплений анализируется с учетом соответствующих механизмов конвективного и лучистого переноса тепла. Быстрым испарением и уменьшением размера относительной доли малых пузырьков можно объяснить экспоненциальную скорость переноса энергии от поверхностного слоя непосредственно над фронтом закалки и по аналогии более высокую интенсивность теплопередачи вниз по течению от преграды.